Supporting Information for

Synergistic doping and structural engineering over dendritic NiMoCu electrocatalyst enabling highly efficient hydrogen production

Ruopeng Li[a], Yang Yuan[a], Haoliang Gui[a], Yaqi Liu[a], Haoyu Li[a], Yaqiang Li[a], Shizheng Wen[c], Anmin Liu[b], Jinqiu Zhang[a], Peixia Yang✉[a] and Maozhong An[a]

This profile includes **Computational details, 17 Figures, 4 Tables, 1 Videos, 22 references.**

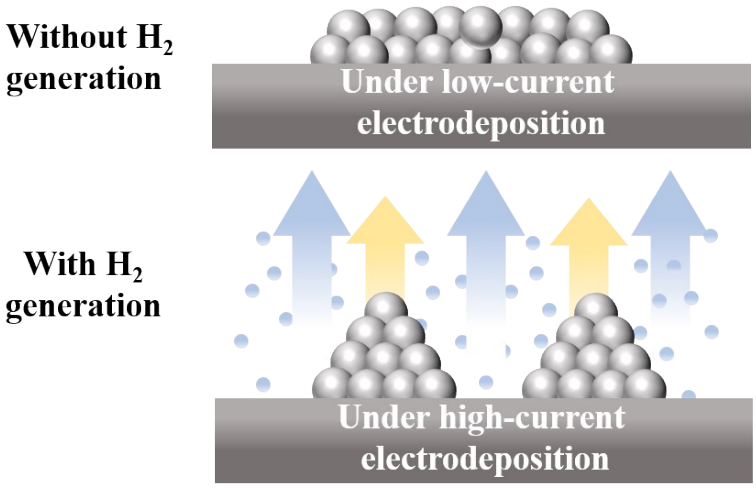

Figure S1 Schematic illustration of gas-template electrodeposition.

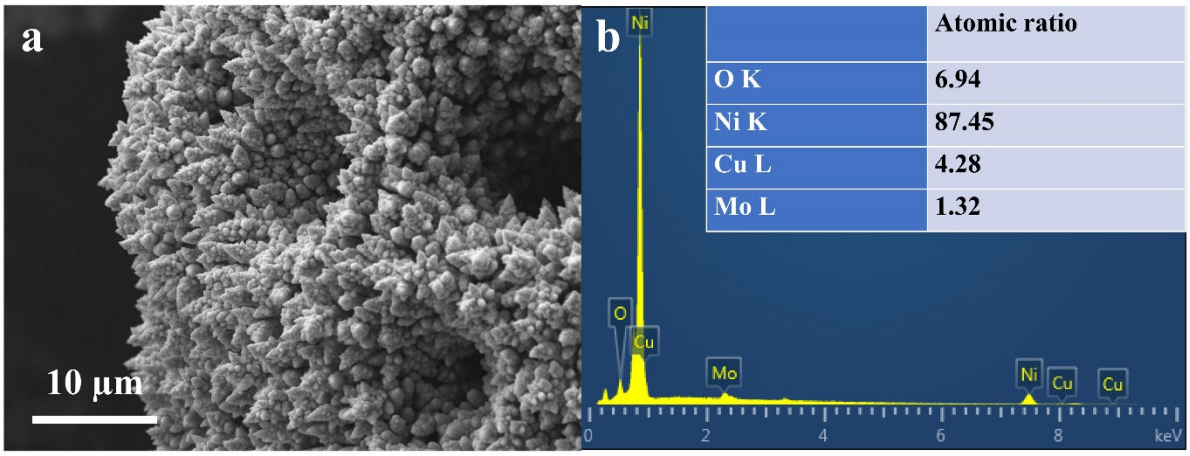

Figure S2 SEM image and EDS analyses of NiMoCu-NF

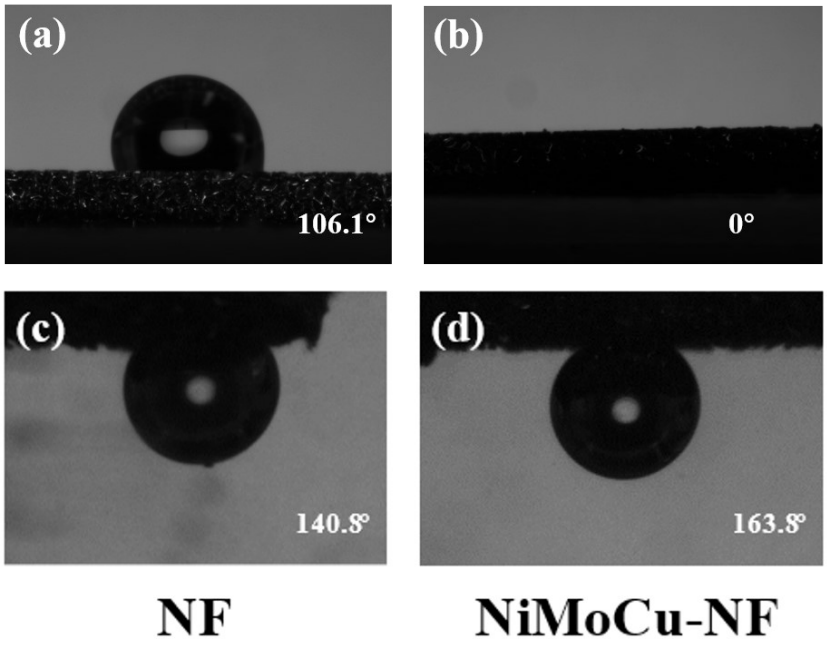

Figure S3 The liquid contact angle (a, b) and gas evolution angle (c, d) images of NF and NiMoCu-NF, respectively.

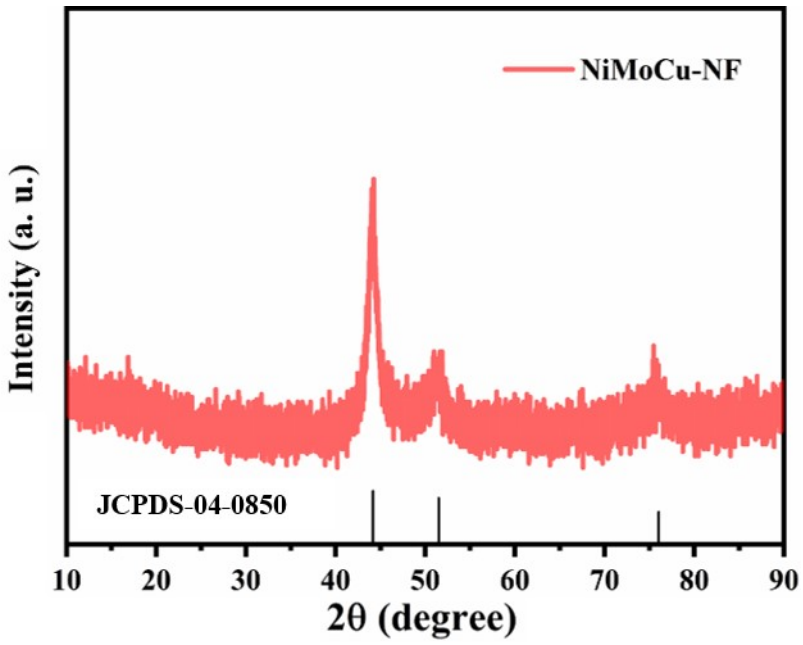

Figure S4 XRD pattern of NiMoCu-NF.

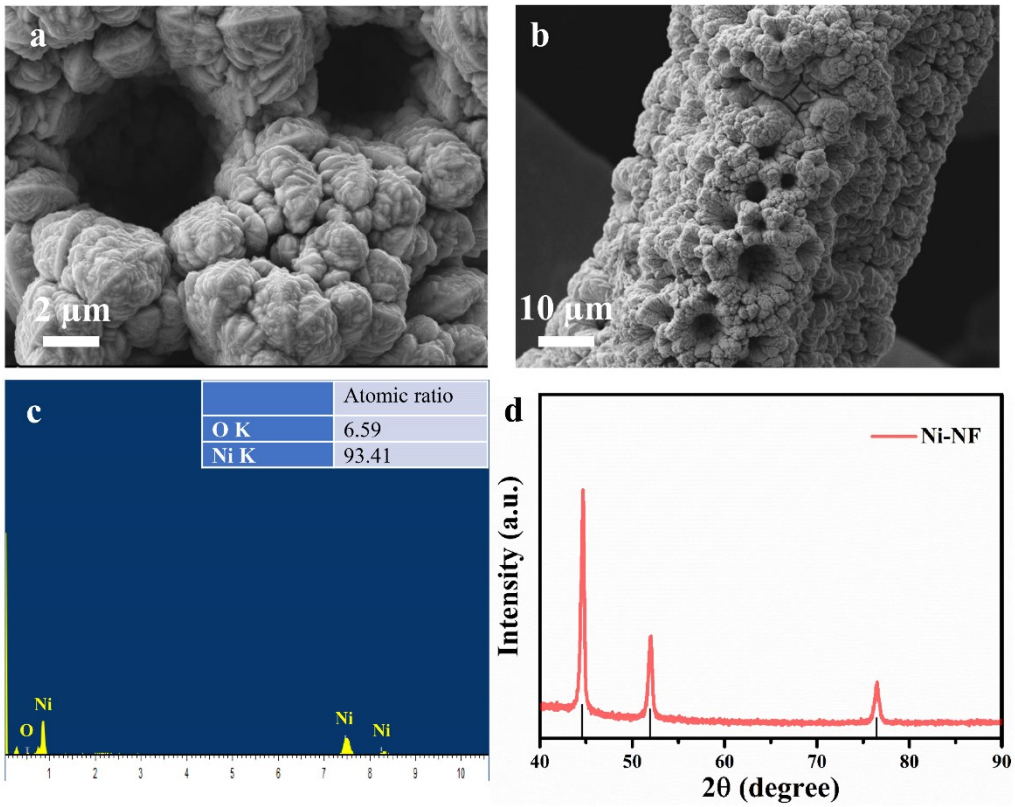

Figure S5 (a) SEM images (b) EDS analysis and (c) XRD pattern of Ni-NF.

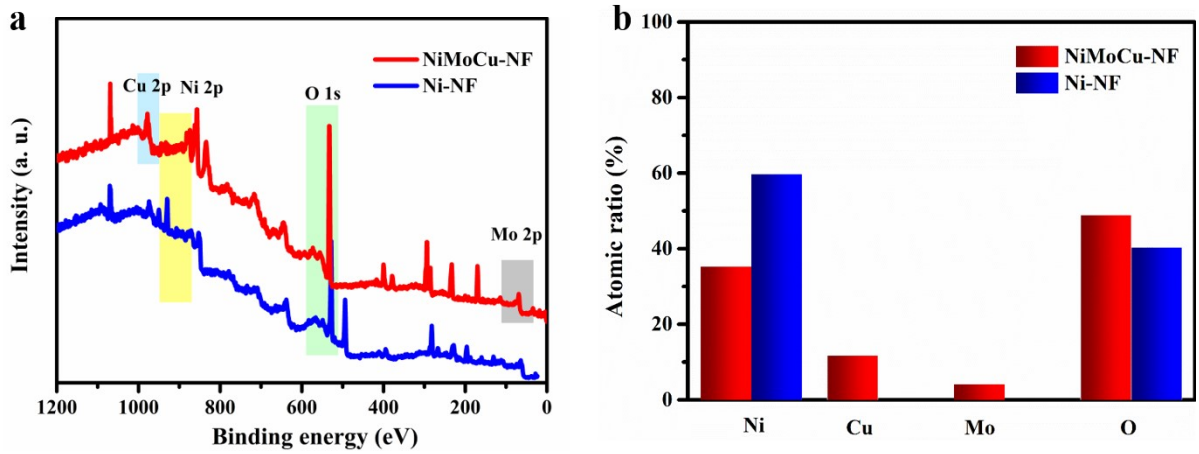

Figure S6 (a) XPS survey spectrum of NiMoCu-NF and Ni-NF. (b) the corresponding element ratio.

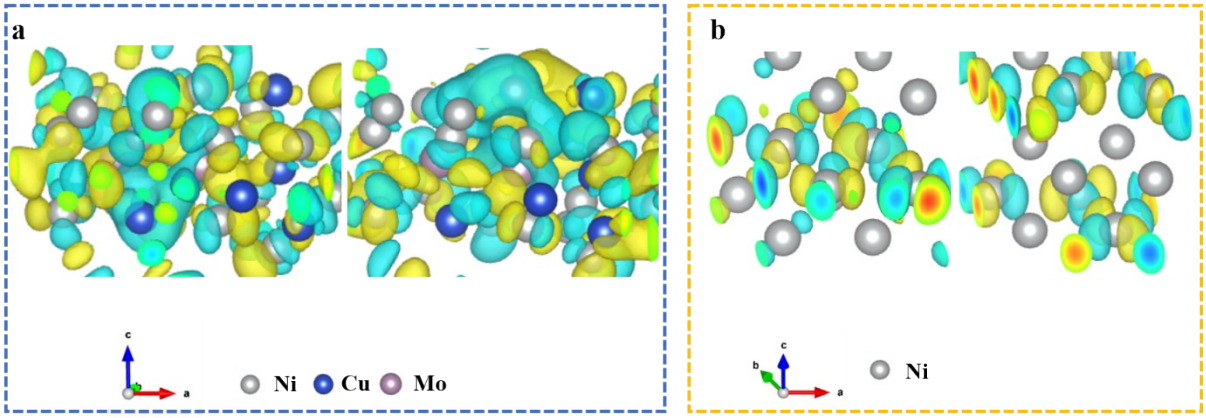

Figure S7 HOMO and LUMO energy barriers of (a) NiMoCu and (b) Ni.

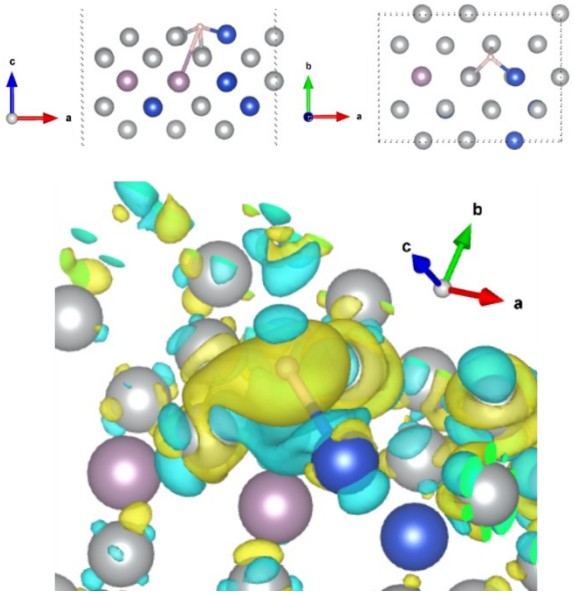

Figure S8 Simulated electron density distribution of NiMoCu-H.

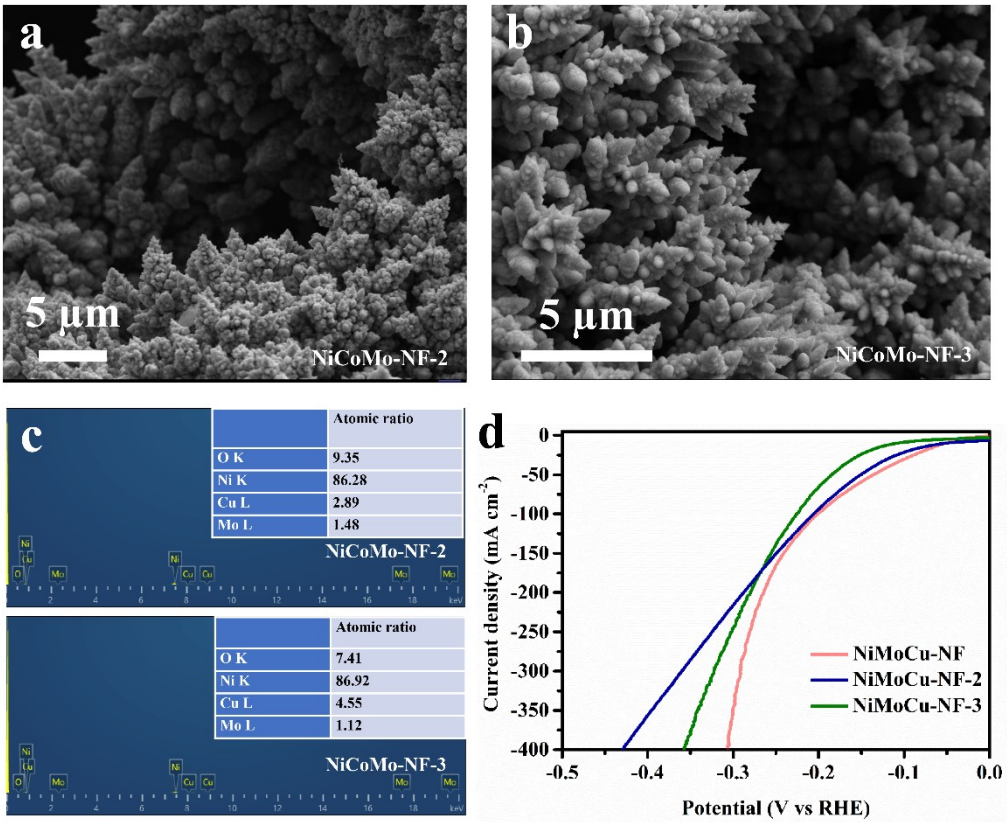

Figure S9 a-c) SEM images and corresponding EDS spectra of NiMoCu-NF-2 and NiMoCu-NF-3. d) LSV curves of NiMoCu-NF, NiMoCu-NF-2 and NiMoCu-NF-3, respectively.

To explore the effect of compositional changes in NiMoCu catalysts, we prepared a control group by changing the ratio of dopant species in the plating solution. (1) Adjust the concentration of molybdate in the plating solution to 1 g L^{-1} and prepare a product, denoted as NiMoCu-NF-2; (2) Adjust the concentration of copper salt in the plating solution to 3 g L^{-1} and prepare a product, denoted as NiMoCu-NF-3.

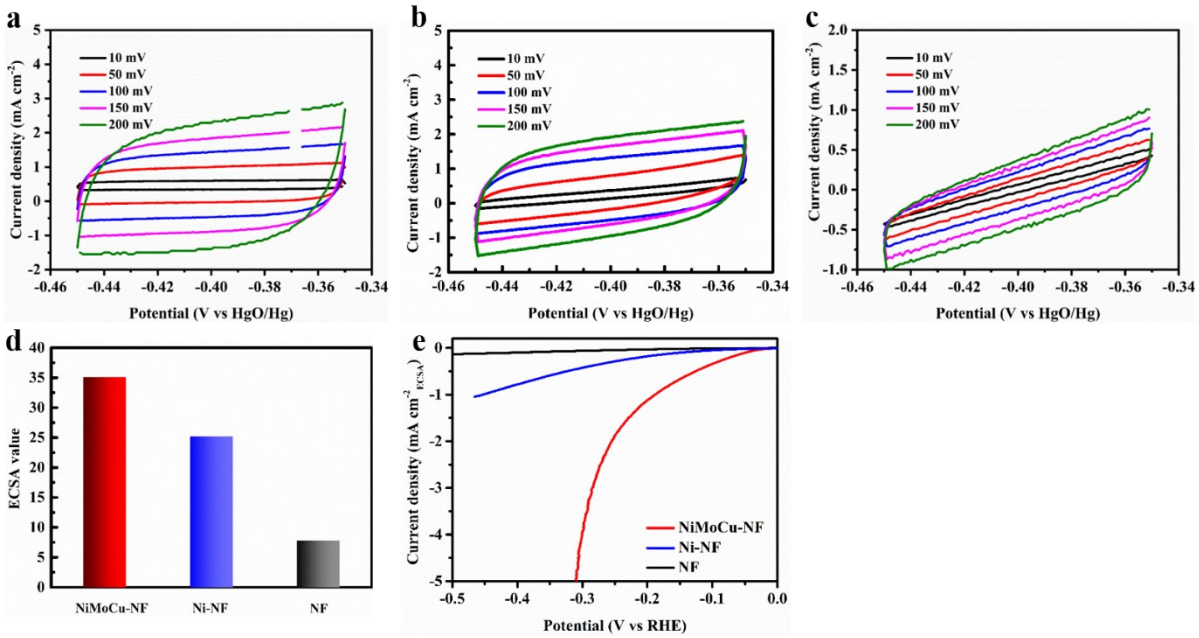

Figure S10 (a-c) CV curves of NiMoCu-NF, Ni-NF and NF in 1 M KOH solution. (d) calculated ECSA values and (e) ECSA normalized LSV curves of the all-prepared samples.

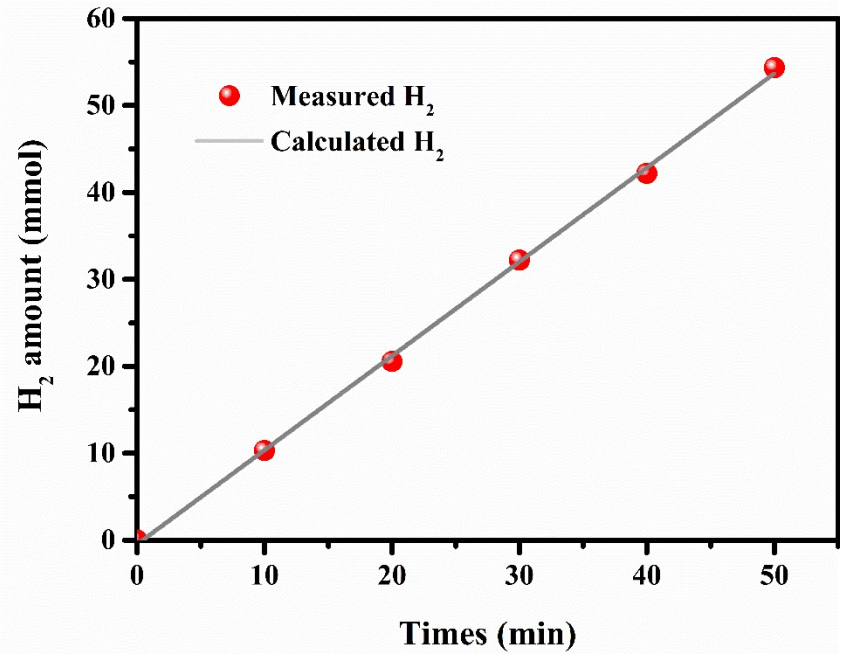

Figure S11 HER Faradaic efficiency (FE) of NiMoCu-NF under 10 mA cm^{-2} measurement.

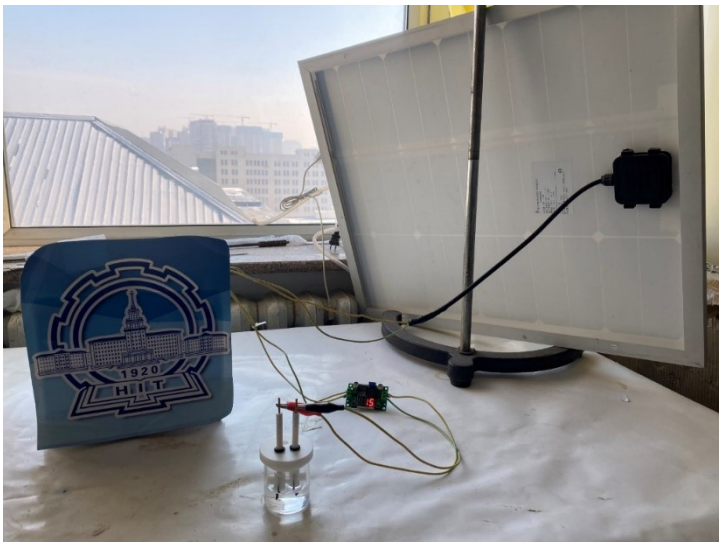

Figure S12 (a) Digital image of the solar-power electrolysis system.

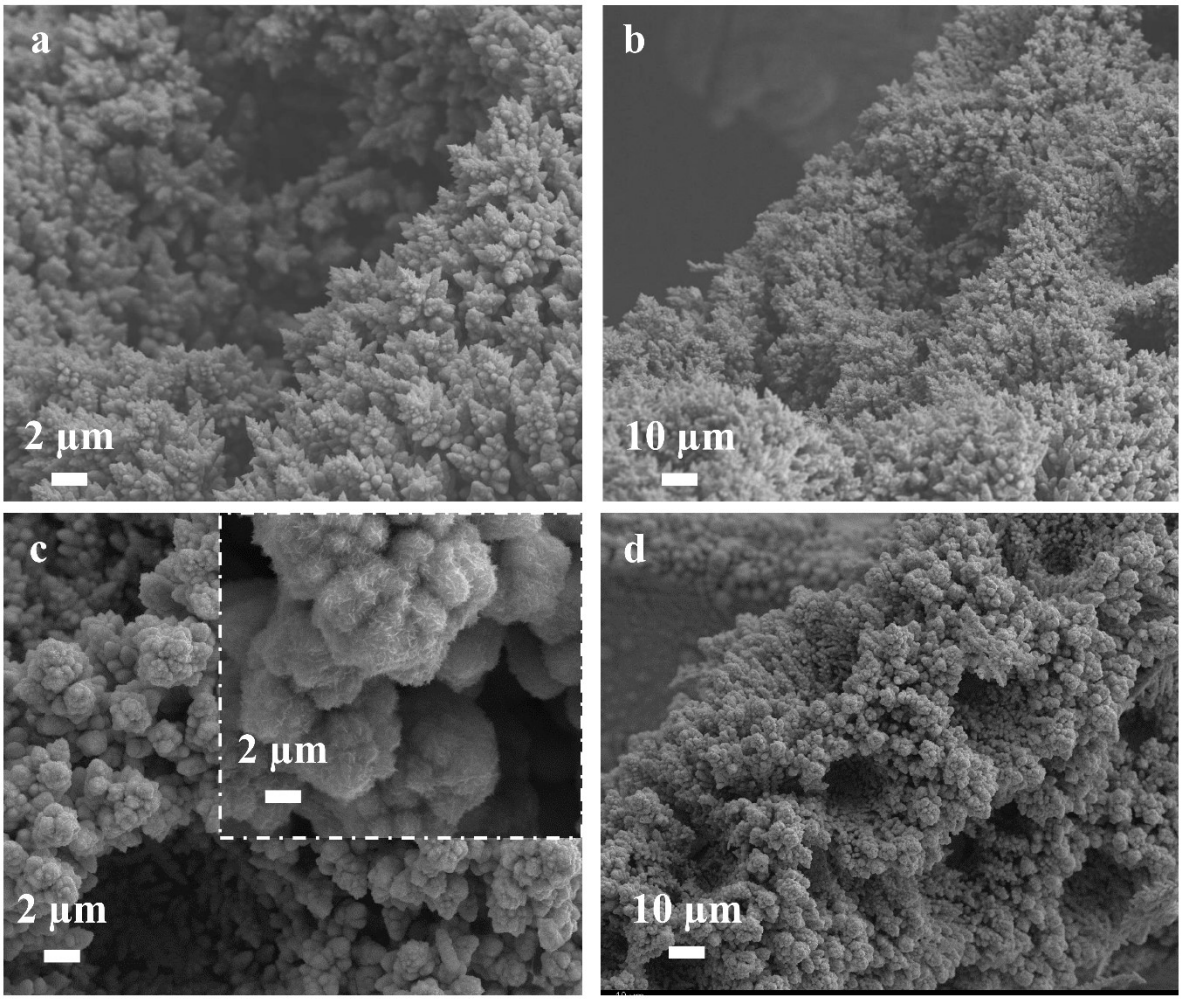

Figure S13 SEM images NiMoCu-NF after long-term stability test of HER (a, b) and UOR (c, d), respectively.

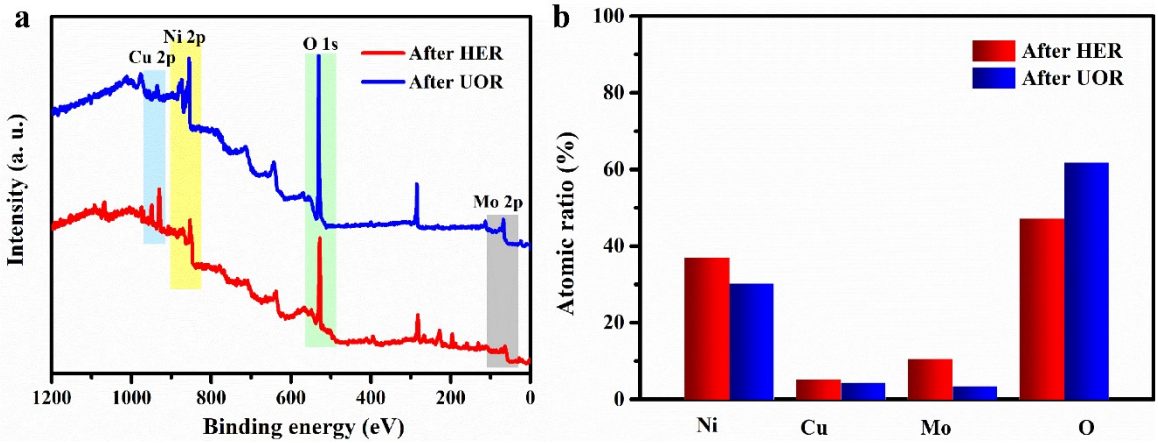

Figure S14. (a, b) XPS survey spectra and the corresponded element ratio of NiMoCu-NF after HER and UOR, respectively.

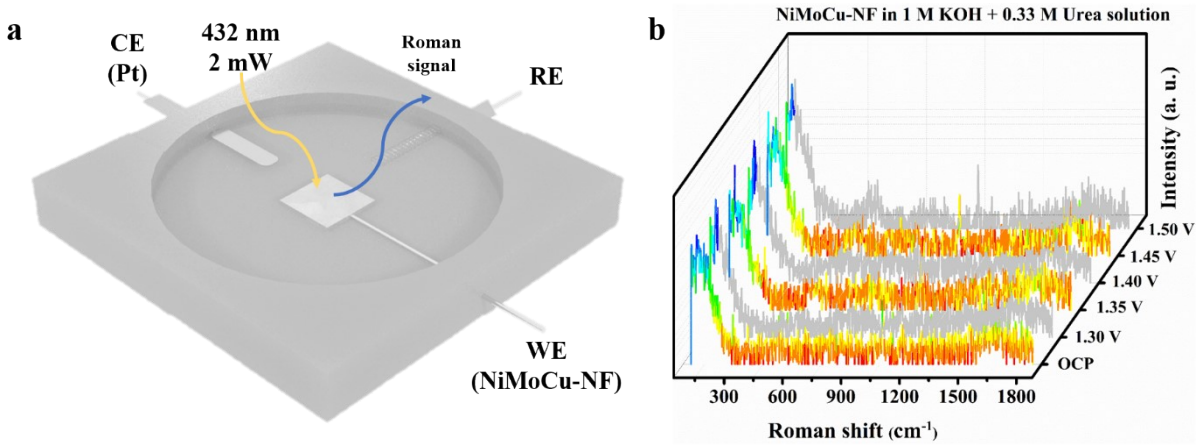

Figure S15. (a) Schematic diagram of the in-situ Raman spectroscopy measurement. (b) In-situ Roman spectra of NiMoCu-NF under oxidizing conditions in 1 M KOH + 0.33 M urea.

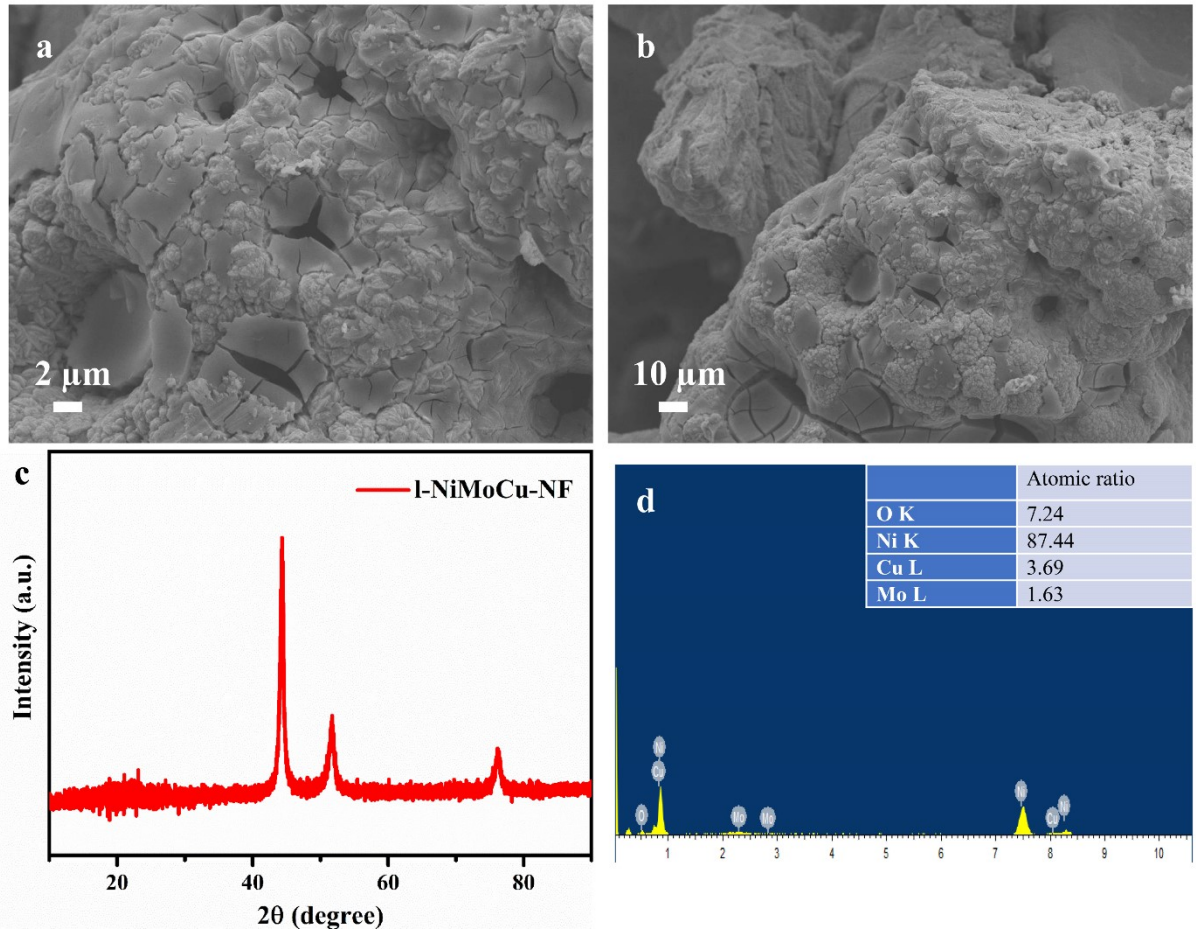

Figure S16. (a, b) SEM images (c) XRD pattern and (d) EDS analysis of l-NiMoCu-NF.

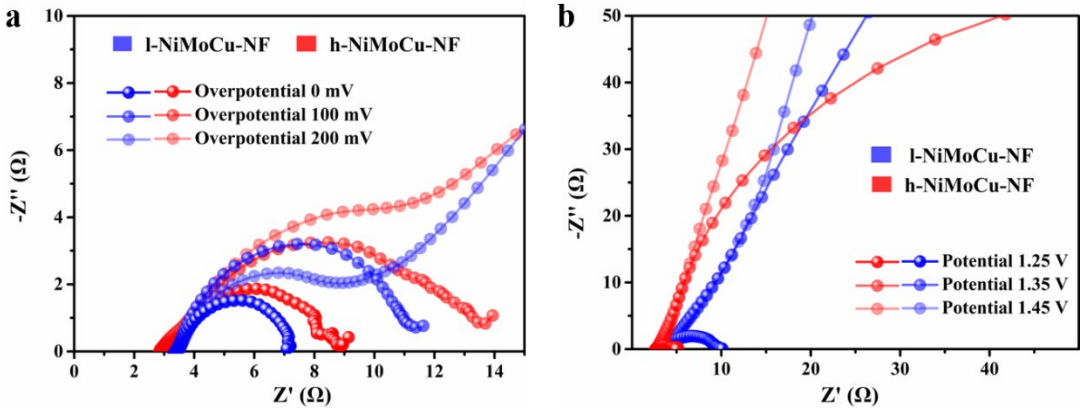

Figure S17. Nuquiest curves comparing NiMoCu-NF and l-NiMoCu-NF of (a) HER and (b) UOR.

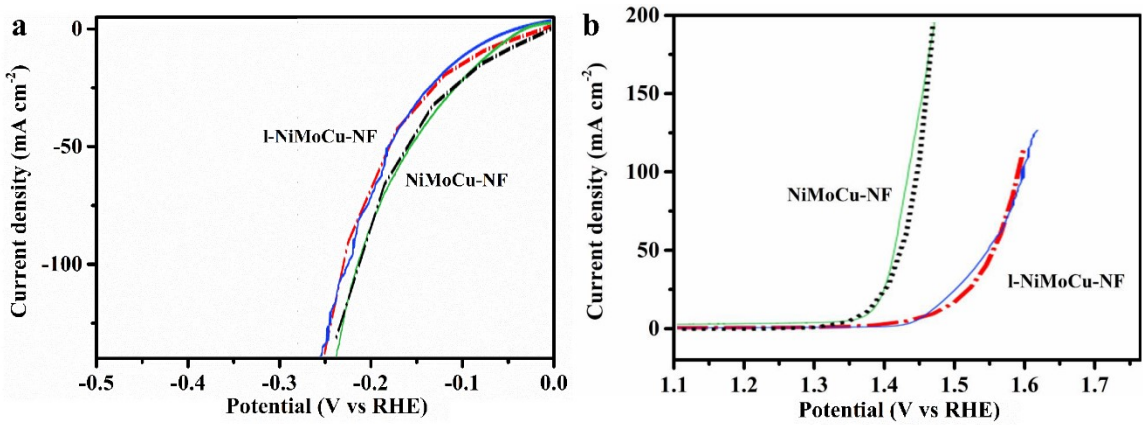

Figure S18. Comparison of simulated and tested LSV curves (a) HER and (b) UOR.

Table S1 ICP analyses of $NiCo(OH)_x$-NF, $NiFe(OH)_x$-NF, and $NiCoFe(OH)_x$-NF

	Ni	Mo	Cu
NiMoCu-NF (Dissolved mass) 4.65 mg cm^{-2}	2.610 mg/L	0.351 mg/L -	0.875 mg/L
Ni-NF (Dissolved mass) 3.37 mg cm^{-2}	2.702 mg/L		-

Table S2. EIS analyses corresponding to Nyquist curves in Figure S11.

	R_{ct} (Ω)	R_{Ω} (Ω)	CPE-T(F)	CPE-P (F)
NiMoCu-NF	1.786	2.778	0.1494	0.6753
Ni-NF	29.633	2.817	0.0029	0.9006
NF	157.5	157.5	0.0010	0.8018

Table S3. The HER potential and Tafel slopes of the non-noble metal-based HER in 1 M KOH solution.

Catalyst	Potential (η_{10})	electrolyte	Tafel slope (mV dec^{-1})	Ref.
NiMoCu-NF	52	1. 0M KOH	52	This Work
$NiSe_2$NTA	60	1.0 M KOH	65	[1]
CoNiMoO NWs	60	1.0 M KOH	73	[2]
CuCoO NWs	85	1.0 M KOH	108	[3]
Ni/NiO−CNT	80	1.0 M KOH	82	[4]
Ni_xB/MWCNT	116	1.0 M KOH	70.4	[5]
O-NiMoP/NF	55	1.0 M KOH	49	[6]
S-NiCu-O(OH)/NF	146	1.0 M KOH	64	[7]
reduced MoS_2	71	1.0 M KOH	100	[8]
$Ni_xCo_{3-x}S_4/Ni_3S_2$	136	1.0 M KOH	107	[9]
Co–P/NF	70	1 M KOH	68	[10]
$Ni-0.2NH_3$	61	1 M KOH	71	[11]
Co–Ni–B NSs	80	1.0 M KOH	88.2	[12]

Table S4. The HER potential and Tafel slopes of the non-noble metal-based HER in 1 M KOH solution.

Catalys	SEM	Electrolyte	Cell Voltage (V) 10 mA cm^{-2}	Ref.
1%Cu:α-$Ni(OH)_2$	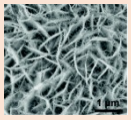	1.0 M KOH 0.33 M urea	1.49	[13]
$Ni(OH)_2$ NS@NW/NF	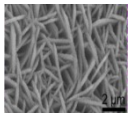	1.0 M KOH 0.33 M urea	1.58	[14]
Ni_9S_8/CuS/Cu_2O /NF	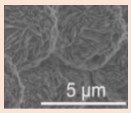	1.0 M KOH 0.33 M urea	1.47	[7]
$NiCo_2S_4$ NS	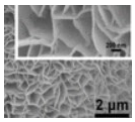	1.0 M KOH 0.33 M urea	1.45	[15]
$Ni_{0.9}Fe_{0.1}O_x$	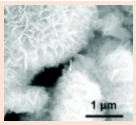	1.0 M KOH 0.33 M urea	1.455	[16]
Ni_3N NA/CC	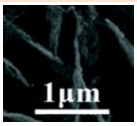	1.0 M KOH 0.33 M urea	1.44	[17]
Ni/C	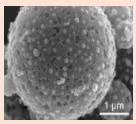	1.0 M KOH 0.33 M urea	1.60	[18]
Ni–Mo nanotube	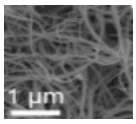	1.0 M KOH 0.5 M urea	1.43	[19]
NiTe/rGO/NF		1.0 M KOH 0.33 M urea	1.5	[20]
Ni_2P/CFC	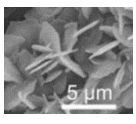	1.0 M KOH 0.33 M urea	1.44	[21]
$Fe_{11.1\%}$–Ni_3S_2/NF	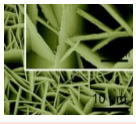	1.0 M KOH 0.33 M urea	1.46	[22]
NiMoCu-NF	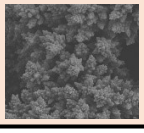	1.0 M KOH 0.33 M urea	1.386	This Work

Movie S1 Liquid contact process of NF.

Movie S2 Liquid contact process of NiMoCu-NF.
Movie S3 NiMoCu -NF || NiMoCu-NF electrolyze driven by a solar-powered system at 1.5 V.

References

[1] X. Teng, J. Wang, L. Ji, Y. Lv, Z. Chen, Ni nanotube array-based electrodes by electrochemical alloying and de-alloying for efficient water splitting, Nanoscale 10(19) (2018) 9276-9285. https://doi.org/10.1039/c8nr02238k.

[2] B. Ren, D. Li, Q. Jin, H. Cui, C. Wang, In-situ Tailoring Cobalt Nickel Molybdenum Oxide Components for Overall Water-Splitting at High Current Densities, Chemelectrochem 6(2) (2019) 413-420. https://doi.org/10.1002/celc.201801386.

[3] M. Kuang, P. Han, Q. Wang, J. Li, G. Zheng, CuCo Hybrid Oxides as Bifunctional Electrocatalyst for Efficient Water Splitting, Advanced Functional Materials 26(46) (2016) 8555-8561. https://doi.org/10.1002/adfm.201604804.

[4] M. Gong, W. Zhou, M.-C. Tsai, J. Zhou, M. Guan, M.-C. Lin, B. Zhang, Y. Hu, D.-Y. Wang, J. Yang, S.J. Pennycook, B.-J. Hwang, H. Dai, Nanoscale nickel oxide/nickel heterostructures for active hydrogen evolution electrocatalysis, Nature Communications 5 (2014). https://doi.org/10.1038/ncomms5695.

[5] X. Chen, Z. Yu, L. Wei, Z. Zhou, S. Zhai, J. Chen, Y. Wang, Q. Huang, H.E. Karahan, X. Liao, Y. Chen, Ultrathin nickel boride nanosheets anchored on functionalized carbon nanotubes as bifunctional electrocatalysts for overall water splitting, Journal of Materials Chemistry A 7(2) (2019) 764-774. https://doi.org/10.1039/c8ta09130g.

[6] H. Jiang, M. Sun, S. Wu, B. Huang, C.-S. Lee, W. Zhang, Oxygen-Incorporated NiMoP Nanotube Arrays as Efficient Bifunctional Electrocatalysts For Urea-Assisted Energy-Saving Hydrogen Production in Alkaline Electrolyte, Advanced Functional Materials 31(43) (2021). https://doi.org/10.1002/adfm.202104951.

[7] D. Wei, W. Tang, Y. Wang, Hairy sphere-like Ni9S8/CuS/Cu2O composites grown on nickel foam as bifunctional electrocatalysts for hydrogen evolution and urea electrooxidation, International Journal of Hydrogen Energy 46(40) (2021) 20950-20960. https://doi.org/10.1016/j.ijhydene.2021.03.206.

[8] M.A.R. Anjum, H.Y. Jeong, M.H. Lee, H.S. Shin, J.S. Lee, Efficient Hydrogen Evolution Reaction Catalysis in Alkaline Media by All-in-One MoS2 with Multifunctional Active Sites, Advanced Materials 30(20) (2018). https://doi.org/10.1002/adma.201707105.

[9] Y. Wu, Y. Liu, G.-D. Li, X. Zou, X. Lian, D. Wang, L. Sun, T. Asefa, X. Zou, Efficient electrocatalysis of overall water splitting by ultrasmall NixCo3-xS4 coupled Ni3S2 nanosheet arrays, Nano Energy 35 (2017) 161-170. https://doi.org/10.1016/j.nanoen.2017.03.024.

[10] M. Song, Z. Zhang, Q. Li, W. Jin, Z. Wu, G. Fu, X. Liu, Ni-foam supported Co(OH)F and Co-P nanoarrays for energy-efficient hydrogen production via urea electrolysis, Journal of

Materials Chemistry A 7(8) (2019) 3697-3703. https://doi.org/10.1039/c8ta10985k.
[11] T. Wang, Q. Zhou, X. Wang, J. Zheng, X. Li, MOF-derived surface modified Ni nanoparticles as an efficient catalyst for the hydrogen evolution reaction, Journal of Materials Chemistry A 3(32) (2015) 16435-16439. https://doi.org/10.1039/c5ta04001a.
[12] M. Sheng, Q. Wu, Y. Wang, F. Liao, Q. Zhou, J. Hou, W. Weng, Network-like porous Co-Ni-B grown on carbon cloth as efficient and stable catalytic electrodes for hydrogen evolution, Electrochemistry Communications 93 (2018) 104-108. https://doi.org/10.1016/j.elecom.2018.06.017.
[13] J. Xie, L. Gao, S. Cao, W. Liu, F. Lei, P. Hao, X. Xia, B. Tang, Copper-incorporated hierarchical wire-on-sheet α-Ni(OH)2 nanoarrays as robust trifunctional catalysts for synergistic hydrogen generation and urea oxidation, Journal of Materials Chemistry A 7(22) (2019) 13577-13584. https://doi.org/10.1039/c9ta02891a.
[14] Z. Yue, S. Yao, Y. Li, W. Zhu, W. Zhang, R. Wang, J. Wang, L. Huang, D. Zhao, J. Wang, Surface engineering of hierarchical Ni(OH)2 nanosheet@nanowire configuration toward superior urea electrolysis, Electrochimica Acta 268 (2018) 211-217. https://doi.org/10.1016/j.electacta.2018.02.059.
[15] W. Zhu, M. Ren, N. Hu, W. Zhang, Z. Luo, R. Wang, J. Wang, L. Huang, Y. Suo, J. Wang, Traditional NiCo2S4 Phase with Porous Nanosheets Array Topology on Carbon Cloth: A Flexible, Versatile and Fabulous Electrocatalyst for Overall Water and Urea Electrolysis, Acs Sustainable Chemistry & Engineering 6(4) (2018) 5011-5020. https://doi.org/10.1021/acssuschemeng.7b04663.
[16] F.C. Wu, G. Ou, J. Yang, H.N. Li, Y.X. Gao, F.M. Chen, Y. Wang, Y.M. Shi, Bifunctional nickel oxide-based nanosheets for highly efficient overall urea splitting, Chemical Communications 55(46) (2019) 6555-6558. https://doi.org/10.1039/c9cc02507c.
[17] Q. Liu, L. Xie, F. Qu, Z. Liu, G. Du, A.M. Asiri, X. Sun, A porous Ni3N nanosheet array as a high-performance non-noble-metal catalyst for urea-assisted electrochemical hydrogen production, Inorganic Chemistry Frontiers 4(7) (2017) 1120-1124. https://doi.org/10.1039/c7qi00185a.
[18] L. Wang, L. Ren, X. Wang, X. Feng, J. Zhou, B. Wang, Multivariate MOF-Templated Pomegranate-Like Ni/C as Efficient Bifunctional Electrocatalyst for Hydrogen Evolution and Urea Oxidation, Acs Applied Materials & Interfaces 10(5) (2018) 4750-4756. https://doi.org/10.1021/acsami.7b18650.
[19] J.-Y. Zhang, T. He, M. Wang, R. Qi, Y. Yan, Z. Dong, H. Liu, H. Wang, B.Y. Xia, Energy-saving hydrogen production coupling urea oxidation over a bifunctional nickel-molybdenum nanotube array, Nano Energy 60 (2019) 894-902. https://doi.org/10.1016/j.nanoen.2019.04.035.

[20] Z. Wang, P. Guo, M. Liu, C. Guo, H. Liu, S. Wei, J. Zhang, X. Lu, Rational Design of Metallic NiTex (x=1 or 2) as Bifunctional Electrocatalysts for Efficient Urea Conversion, Acs Applied Energy Materials 2(5) (2019) 3363-3372. https://doi.org/10.1021/acsaem.9b00208.
[21] L. Xie, Q. Liu, Y. Luo, Z. Liu, Y. Xu, A.M. Asiri, X. Sun, F. Xie, Bimetallic NiCoP Nanosheets Array for High-Performance Urea Electro-Oxidation and Less Energy-Intensive Electrolytic Hydrogen Production, Chemistryselect 2(31) (2017) 10285-10289. https://doi.org/10.1002/slct.201702071.
[22] W. Zhu, Z. Yue, W. Zhang, N. Hu, Z. Luo, M. Ren, Z. Xu, Z. Wei, Y. Suo, J. Wang, Wet-chemistry topotactic synthesis of bimetallic iron-nickel sulfide nanoarrays: an advanced and versatile catalyst for energy efficient overall water and urea electrolysis, Journal of Materials Chemistry A 6(10) (2018) 4346-4353. https://doi.org/10.1039/c7ta10584c.